Available online at www.sciencedirect.com
SCIENCE DIRECT®
ELSEVIER
Coastal Engineering 48 (2003) 257–275
Coastal Engineering
An International Journal for Coastal, Harbour and Offshore Engineers
www.elsevier.com/locate/coastaleng

An unsteady wave driver for narrowbanded waves: modeling nearshore circulation driven by wave groups

Andrew B. Kennedy[a,*], James T. Kirby[b]

[a] Department of Civil and Coastal Engineering, University of Florida, Gainesville, FL 32611-6590, USA
[b] Center for Applied Coastal Research, University of Delaware, Newark, DE 19716, USA

Received 17 June 2002; received in revised form 1 April 2003; accepted 12 May 2003

Abstract

In this paper, we derive an unsteady refraction–diffraction model for narrowbanded water waves for use in computing coupled wave–current motion in the nearshore. The end result is a variable coefficient, nonlinear Schrödinger-type wave driver (describing the envelope of narrow-banded incident waves) coupled to forced nonlinear shallow water equations (describing steady or unsteady mean flows driven by the short-wave field). Comparisons with experimental data show that good accuracy can be obtained for cases of nonbreaking wave transformation. Numerical simulations show that the interaction of wave groups with longshore topographic nonuniformities generates strong edge wave resonances, providing a generating mechanism for low-order edge waves.

Keywords: Water waves; Wave transformation; Numerical methods; Nearshore circulation; Diffraction; Edge waves

1. Introduction

Surface waves breaking nearshore generate a wide range of steady and unsteady motions, resulting from a forcing mechanism associated with spatial and temporal variations in wave-induced momentum fluxes or radiation stresses (Longuet-Higgins and Stewart, 1964). The existence of the radiation stress formulation has led to a long history of development of nearshore circulation models in which wave and current processes are separated through a suitable time average and treated separately, with or without feedback of current information. The wave field is computed using a suitable *wave driver*, which calculates a representative wave field in some fashion and derives the radiation stress forcing, and a *circulation model*, which uses the radiation stress forcing to drive a steady or quasi-steady (when compared to the wave time scale) circulation. Recent examples of this type of modeling application range from narrowly defined process studies (Allen et al., 1996; Özkan-Haller and Kirby, 1999) to fully documented modeling systems aimed at general application (Svendsen et al., 2002, for example).

Steady forcing resulting from monochromatic waves can lead to a range of motions including steady longshore currents (Bowen, 1969a) or, especially in

* Corresponding author.
E-mail addresses: kennedy@coastal.ufl.edu (A.B. Kennedy), kirby@udel.edu (J.T. Kirby).

0378-3839/03/$ - see front matter © 2003 Elsevier B.V. All rights reserved.
doi:10.1016/S0378-3839(03)00031-0

the presence of perturbed bottom configurations, rip currents and circulation cells (Bowen, 1969b; Dalrymple and Lozano, 1978). These motions may themselves be steady, or they may evolve through a variety of instability mechanisms (Bowen and Holman, 1989; Haller and Dalrymple, 2001) into unsteady motions with periodic, quasi-periodic or chaotic behavior (Allen et al., 1996; Chen et al., 1999). For field conditions, the forcing resulting from the shoaling and breaking of broadbanded spectral sea states is often represented in terms of a time average over a number of waves in order to obtain a quasi-stationary estimate of forcing. Thus, aside from a smearing of the break point due to the probabilistic nature of individual wave breaking events, the forcing conditions in broadbanded seas are treated in a manner which is qualitatively similar to the approach for monochromatic waves, providing a steady driving term for stationary spectral sea states. The range of motions resulting from this extension to the theory is thus also qualitatively similar to the monochromatic case since they are not tied to any apparent or implied time scales in the incident wave field.

In contrast, wave fields with narrowbanded frequency structure have pronounced groupiness, or variation of wave height on time scales slower than the dominant wave period. Pronounced groupiness leads to a concurrent pronounced variation in radiation stress forcing with time scales typically of O(100 s), leading to a variety of infragravity motions in the nearshore, including surf beat (Schäffer, 1993) and edge waves (Gallagher, 1971; Schäffer, 1994; Lippmann et al., 1997). These motions can be predicted for broad spectral sea states as well, but it becomes unclear whether the resulting motions are to be represented as part of the wave field or circulation field in the modeling systems.

For the case of monochromatic waves, Stokes theory has often provided a successful approach to the derivation of the wave driver. The leading order approximation provides the familiar mild slope equation (Berkhoff, 1972) and its forward-scattering approximations, usually based on the parabolic equation method (Radder, 1979; Lozano and Liu, 1980). Extending the Stokes theory to third order, Kirby and Dalrymple (1983) derived a model for periodic wave propagation over variable depth in the form of a cubic Schrödinger equation and verified the resulting model in comparison to laboratory data (Berkhoff et al., 1982) for the case of wave propagation over a submerged shoal (Kirby and Dalrymple, 1984). The inclusion of wave–current interaction effects and the extension of the parabolic equation formulation to allow a larger range of incident wave angles are described by Kirby (1986). Kirby and Dalrymple (1986) treated the singularity in Stokes theory in the limit of small water depth using an empirical modification to the cubic Schrödinger nonlinear term to be described below, where the cubic term is replaced by an empirical term mimicking shallow water phase speed corrections. These modifications to the original theory have produced a robust model for computing monochromatic, phase-resolved wave refraction, shoaling, diffraction and breaking in the nearshore. The resulting model (or others of similar form) serves as the wave driver in a number of circulation models, including the SHORECIRC model of Svendsen et al. (2002) mentioned above.

The theoretical basis for a wave driver for groupy, narrowbanded waves, using the Stokes theory and leading to a time-dependent, extended cubic Schrödinger equation at third order, has existed for a number of years, but no practical modeling codes have been documented or introduced for standard usage. The purpose of the present paper is to describe the derivation of a propagation model for unsteady, narrow frequency band waves which is suitable for use as a wave driver for nearshore circulation modeling. The model is capable of handling interaction with a variable bathymetry and current field, to which it is coupled through spatially and temporally varying radiation stress forcing. The model is an extension of the nonlinear Davey and Stewartson (1974) equation, or nonlinear Schrödinger (NLS) equation extended to two horizontal dimensions, coupled to a forced long-wave equation. In application, the simple long-wave model given by the derivation here is replaced by any of a number of models for wave-driven circulation, most of which are formulated in terms of nonlinear long-wave equations with suitable modifications for bottom friction, wave forcing, turbulent mixing and dispersive effects of three-dimensional current structure. The semi-empirical extension of Kirby and Dalrymple (1986) is included to modify wave nonlinearity in shallow water in order to eliminate the singularity in Stokes theory in the limit of shallow water.

In the following derivation, the current and slowly varying water level are specifically treated as $O(1)$ quantities. This approach was pioneered in the context of Schrödinger equations by Foda and Mei (1981), who studied the resonant growth of surf beat driven by shoaling wave groups, and by Turpin et al. (1983), who examined the evolution of wave groups in the presence of strong wave–current interaction. The model is formulated in terms of a modulated carrier wave propagating along rays defined by linear refraction theory, following the original formulation of Chu and Mei (1970); similar results for the case with no strong currents have been presented by Liu and Dingemans (1989). The present derivation parallels that of Liu and Dingemans in many respects, but extends the formulation to include wave–current interaction effects.

A discussion of the governing equations and scaling arguments is given in Section 2, followed by a description of the derivation in Section 3. A brief description of the numerical scheme being used at present is given in Section 4. An example of application of the model in a steady, periodic wave case is given in Section 5. Section 6 examines edge wave generation through the interaction of wave groups with topographic longshore irregularities. Subsequent papers are to examine such topics as the influence of wave groups on mean and fluctuating properties in rip currents.

2. Governing equations and scaling

We begin by assuming potential flow for both the wave and current motion. The fluid velocity vector is defined by a velocity potential ϕ according to $(u, v, w) \equiv \nabla^{(3)}\phi(x, y, t)$, where $\nabla^{(3)} \equiv (\partial/\partial x, \partial/\partial y, \partial/\partial z)$. The potential satisfies Laplace's equation

$$\nabla^{(3)2}\phi = 0, \quad -h \leq z \leq \eta \tag{1}$$

where $h(x, y)$ is the still water depth and $\eta(x, y, t)$ is the free surface elevation.

For a solid bottom boundary, a tangential flow condition must be satisfied

$$\nabla h \cdot \nabla\phi + \phi_z = 0, \quad z = -h \tag{2}$$

where $\nabla \equiv (\partial/\partial x, \partial/\partial y)$.

The free surface elevation's position in time is governed by a kinematic condition

$$\eta_t + \nabla\eta \cdot \nabla\phi - \phi_z = 0, \quad z = \eta \tag{3}$$

or, equivalently, by using Eqs. (1) and (2)

$$\eta_t + \nabla \cdot \int_{-h}^{\eta} \nabla\phi \mathrm{d}z = 0 \tag{4}$$

The evolution of fluid velocity is governed by an unsteady form of Bernoulli's equation

$$\phi_t + g\eta + \frac{1}{2}(\phi_x^2 + \phi_y^2 + \phi_z^2) = 0, \quad z = \eta \tag{5}$$

where g is the downwards positive gravitational forcing.

The two surface conditions may be combined to give a single evolution equation

$$\phi_{tt} + g\phi_z + \left[\frac{\partial}{\partial t} + \frac{1}{2}\nabla\phi \cdot \nabla + \frac{1}{2}\phi_z\frac{\partial}{\partial z}\right] \times \left[\phi_x^2 + \phi_y^2 + \phi_z^2\right] = 0, \quad z = \eta \tag{6}$$

Now, we explicitly separate the flow field and free surface into wave and current portions, $\phi = \phi_\mathrm{w} + \phi_\mathrm{c}$, $\eta = \eta_\mathrm{w} + \eta_\mathrm{c}$. The time evolution of the long-wave quantities $(\eta_\mathrm{c}, \phi_\mathrm{c})$ are to come from the current portion of the model, which could be anyone of a number of existing models. Since these models invariably do *not* expand quantities in terms of amplitude, we will do likewise. This is to say that we will assume that $(\eta_\mathrm{c}, \nabla\phi_\mathrm{c})$ are $O(1)$ quantities and do not have series expansions in terms of their amplitudes. (We will, however, expand ϕ_c dispersively about the long-wave limit at one point.)

As the full unsteady problem is intractable for any reasonably sized domain, we now make scaling assumptions based on a knowledge of the various components of the flow. To decide which terms to keep or omit, we will briefly switch to dimensionless variables, but will soon revert to dimensional quantities for the remainder of this paper.

The wave portion of the flow is subject to standard Stokes scaling,

$$x = k_\mathrm{s}x^*, \quad y = k_\mathrm{s}y^*, \quad z = k_\mathrm{s}z^*, \quad \eta_\mathrm{w} = \frac{\eta_\mathrm{w}^*}{a},$$
$$\phi_\mathrm{w} = \frac{k_\mathrm{s}\phi_\mathrm{w}^*}{a\sqrt{gk_\mathrm{s}}}, \quad t = \sqrt{gk_\mathrm{s}}t^* \tag{7}$$

where k_s is a typical wave number, a is a typical wave amplitude and superscripts here indicate dimensional quantities.

The current portion of the flow follows shallow water scaling, with quantities scaled by a typical wave number, k_0, and water depth, h_0:

$$X = k_0 x^*, \quad Y = k_0 y^*, \quad Z = z^*/h_0, \quad \zeta_c = \eta^*/h_0,$$
$$\Phi_c = \phi_c^* \left(\frac{\sqrt{gh_0}}{k_0}\right)^{-1}, \quad T = t^*\sqrt{gk_0}, \quad H = h^*/h_0 \tag{8}$$

We should thus note explicitly that the dimensionless current and wave portions of the equations use different variable definitions. However, since we are only using the dimensionless equations for order of magnitude estimates and will revert to dimensional quantities as soon as this is complete, we will not let this worry us.

Introducing the nonlinear parameter, $\epsilon \equiv k_s a$, a dispersive parameter $\mu \equiv k_0 h_0$ and defining a relationship between the two typical wave numbers, $k_0 = \nu k_s$, we arrive at a dimensionless equation for the free surface evolution. For greater clarity, we will present these equations in one horizontal dimension only, as these show all features of interest for order of magnitude considerations, but are considerably less complex.

After dividing by a common factor, we get

$$\begin{aligned}
&\left(\epsilon\phi_{wtt} + \sqrt{\frac{\mu}{\nu}}\mu\Phi_{cTT}\right) + \left(\epsilon\phi_{wz} + \sqrt{\frac{\mu}{\nu}}\frac{1}{\mu}\Phi_{cZ}\right) \\
&\quad + 2\left(\sqrt{\frac{\mu}{\nu}}\mu\Phi_{cX}\Phi_{cXT} + \mu\epsilon\Phi_{cXT}\phi_{wx} + \sqrt{\frac{\mu}{\nu}}\Phi_{cZ}\Phi_{cZT}\right. \\
&\quad \left. + \epsilon\Phi_{cZT}\phi_{wz}\right) + 2\left[\left(\sqrt{\frac{\mu}{\nu}}\Phi_{cX} + \epsilon\phi_{wx}\right)\epsilon\phi_{wxt}\right. \\
&\quad \left. + \left(\frac{1}{\sqrt{\mu\nu}}\Phi_{cZ} + \epsilon\phi_{wz}\right)\epsilon\phi_{wzt}\right] + \left(\sqrt{\frac{\mu}{\nu}}\Phi_{cX} + \epsilon\phi_{wx}\right) \\
&\quad \times \left[\left(\sqrt{\frac{\mu}{\nu}}\Phi_{cX} + \epsilon\phi_{wx}\right)\left(\sqrt{\mu\nu}\Phi_{cXX} + \epsilon\phi_{wxx}\right)\right. \\
&\quad \left. + \left(\frac{1}{\sqrt{\mu\nu}}\Phi_{cZ} + \epsilon\phi_{wz}\right)\left(\sqrt{\frac{\nu}{\mu}}\Phi_{cXZ} + \epsilon\phi_{wxz}\right)\right] \\
&\quad + \left(\frac{1}{\sqrt{\mu\nu}}\Phi_{cZ} + \epsilon\phi_{wz}\right)\left[\left(\sqrt{\frac{\mu}{\nu}}\Phi_{cX} + \epsilon\phi_{wx}\right)\right. \\
&\quad \times \left(\sqrt{\frac{\nu}{\mu}}\Phi_{cXZ} + \epsilon\phi_{wxz}\right) + \left(\frac{1}{\sqrt{\mu\nu}}\Phi_{cZ} + \epsilon\phi_{wz}\right) \\
&\quad \left. \times \left(\frac{1}{\mu}\sqrt{\frac{\nu}{\mu}}\Phi_{cZZ} + \epsilon\phi_{wzz}\right)\right] = 0, \\
&Z + z = \zeta_c + \epsilon\eta_w
\end{aligned} \tag{9}$$

Looking ahead, we will now borrow some well-known results from long-wave theory (e.g. Nwogu, 1993, Eqs. (18) and (20)) for the magnitudes of the current components

$$\begin{aligned}
\Phi_{cX} &= \Phi_{cX}^{(0)} + O(\mu^2) \\
\Phi_{cZ} &= \mu^2\Phi_{cZ}^{(2)} + O(\mu^4) \\
&= -\mu^2[(Z+H)\phi_{cX}^{(0)}]_X + O(\mu^4) \\
\Phi_{cXZ} &= O(\mu^2) \\
\Phi_{cZZ} &= \mu^2\Phi_{cZZ}^{(2)} + O(\mu^4) \\
&= -\mu^2\Phi_{cXX}^{(0)} + O(\mu^4)
\end{aligned} \tag{10}$$

where $\Phi_c^{(0)}$ is the long-wave velocity potential at the bed. This will allow us to discard some terms now that otherwise would have to be carried further in the derivation. These results (Eq. (10)) will be verified later.

All that is left is to relate the various independent nonlinear and dispersive scaling parameters. We assume

$$O(\mu) = O(\nu) = O(\epsilon^2) \tag{11}$$

This assumes that nonlinearity is mild, and long waves are two orders of magnitude longer than the short waves.

With these scaling assumptions, and dropping the superscript on $\Phi_{cX}^{(0)}$, the ordered dimensionless equations become

$$\begin{aligned}
&\epsilon[\phi_{wtt} + \phi_{wz} + 2\Phi_{cX}\phi_{wxt} + \Phi_{cX}^2\phi_{wxx}] + \epsilon^2[2\phi_{wx}\phi_{wxt} \\
&\quad + 2\phi_{wz}\phi_{wzt}] + \epsilon^2[2\Phi_{cX}(\phi_{wx}\phi_{wxx} + \phi_{wz}\phi_{wxz})] \\
&\quad + \epsilon^2[\Phi_{cTT} + \Phi_{cz} + 2\Phi_{cX}\Phi_{cXT} + \Phi_{cX}^2\Phi_{cXX}] \\
&\quad + \epsilon^3[2\Phi_{cZ}^{(2)}\phi_{wzt} + 2\Phi_{cXT}\phi_{wx} + 2\Phi_{cX}\Phi_{cXX}\phi_{wx} \\
&\quad + 2\Phi_{cZ}^{(2)}\Phi_{cX}\phi_{wxz}] + \epsilon^3[\phi_{wx}(\phi_{wx}\phi_{wxx} + \phi_{wz}\phi_{wxz}) \\
&\quad + \phi_{wz}(\phi_{wx}\phi_{wxx} + \phi_{wz}\phi_{wzz})] = 0, \\
&Z + z = \zeta_c + \epsilon\eta_w
\end{aligned} \tag{12}$$

keeping terms up to $O(\epsilon^3)$.

Expanding to two horizontal dimensions and reverting to dimensional variables, but keeping the ordering, we arrive at

$$\epsilon[\Gamma\phi_{\mathrm{w}}]+\epsilon^{2}[D(\nabla^{(3)}\phi_{\mathrm{w}}\cdot\nabla^{(3)}\phi_{\mathrm{w}})+\Gamma\phi_{\mathrm{c}}] + \epsilon^{3}[2\phi_{cz}^{(2)}D\phi_{\mathrm{w}z}+2D_{\mathrm{c}}(\nabla\phi_{\mathrm{c}}\cdot\nabla\phi_{\mathrm{w}})+\nabla^{(3)}\phi_{\mathrm{w}}\cdot\nabla^{(3)} \times(\nabla^{(3)}\phi_{\mathrm{w}}\cdot\nabla^{(3)}\phi_{\mathrm{w}})]=0,\quad z=\eta_{\mathrm{c}}+\eta_{\mathrm{w}} \tag{13}$$

where differential operators

$$D\equiv\partial/\partial t+\nabla\phi_{\mathrm{c}}\cdot\nabla \tag{14}$$

and

$$\Gamma\equiv D^{2}+g\partial/\partial z$$

$$=\frac{\partial^{2}}{\partial t^{2}}+2\left(\phi_{\mathrm{c}x}\frac{\partial^{2}}{\partial x\partial t}+\phi_{\mathrm{c}y}\frac{\partial^{2}}{\partial y\partial t}\right)+\phi_{\mathrm{c}x}^{2}\frac{\partial^{2}}{\partial x^{2}} +2\phi_{\mathrm{c}x}\phi_{\mathrm{c}y}\frac{\partial^{2}}{\partial x\partial y}+\phi_{\mathrm{c}y}^{2}\frac{\partial^{2}}{\partial y^{2}}+g\frac{\partial}{\partial z} \tag{15}$$

The subscript in D_{c} means that the operator only operates on the current portion of the argument.

The system may then be expanded in a Taylor series about the long-wave water level, η_{c}.

$$\phi\mid_{z=\eta_{\mathrm{c}}+\eta_{\mathrm{w}}}=\phi\mid_{z=\eta_{\mathrm{c}}}+\epsilon\eta_{\mathrm{w}}\phi_{z}\mid_{z=\eta_{\mathrm{c}}}+\epsilon^{2}\frac{\eta_{\mathrm{w}}^{2}}{2}\phi_{zz}\mid_{z=\eta_{\mathrm{c}}} +O(\epsilon^{3}) \tag{16}$$

to arrive at

$$\epsilon[\Gamma_{\mathrm{w}}\phi_{\mathrm{w}}]+\epsilon^{2}[D(\nabla^{(3)}\phi_{\mathrm{w}}\cdot\nabla^{(3)}\phi_{\mathrm{w}})+\Gamma\phi_{\mathrm{c}} +\eta_{\mathrm{w}}\Gamma_{\mathrm{w}}\phi_{\mathrm{w}z}]+\epsilon^{3}\Big[2\phi_{\mathrm{c}z}^{(2)}D\phi_{\mathrm{w}z}+2D_{\mathrm{C}}(\nabla\phi_{\mathrm{c}}\cdot\nabla\phi_{\mathrm{w}}) +\nabla^{(3)}\phi_{\mathrm{w}}\cdot\nabla^{(3)}(\nabla^{(3)}\phi_{\mathrm{w}}\cdot\nabla^{(3)}\phi_{\mathrm{w}})+g\eta_{\mathrm{w}}\phi_{\mathrm{c}zz} +\frac{\eta_{\mathrm{w}}^{2}}{2}\Gamma_{\mathrm{w}}\phi_{\mathrm{w}zz}+\eta_{\mathrm{w}}D(2\nabla^{(3)}\phi_{\mathrm{w}z}\cdot\nabla^{(3)}\phi_{\mathrm{w}})\Big]=0, \quad z=\eta_{\mathrm{c}} \tag{17}$$

To remove the free surface entirely from the system, Eq. (5) is then used. After some order of magnitude calculations similar to those previous, and making use of Eq. (16), we arrive at

$$\eta_{\mathrm{c}}+\epsilon\eta_{\mathrm{w}} =-\frac{1}{g}\left[\phi_{\mathrm{c}t}+\frac{1}{2}(\phi_{\mathrm{c}x}^{2}+\phi_{\mathrm{c}y}^{2})\right] -\epsilon\frac{1}{g}[\phi_{\mathrm{w}t}+\nabla\phi_{\mathrm{c}}\cdot\nabla\phi_{\mathrm{w}}] -\epsilon^{2}\frac{1}{g}\left[-\frac{1}{g}\phi_{\mathrm{w}t}\phi_{\mathrm{w}zt}+\frac{1}{2}(\nabla^{(3)}\phi_{\mathrm{w}}\cdot\nabla^{(3)}\phi_{\mathrm{w}})\right] +O(\epsilon^{3}),\quad z=\eta_{\mathrm{c}}. \tag{18}$$

3. Derivation of evolution equations by multiple scales

We proceed using the multiple-scale approach following Chu and Mei (1970) and subsequent investigators. The dimensions x, y, t are expanded in the form $(x,y)=(x,y)+\epsilon(X_1,Y_1)+\epsilon^2(X_2,Y_2)+\ldots$, $t=t+\epsilon T_1+\epsilon^2T_2+\ldots$. This applies to all equations, including the continuity condition, the bottom boundary condition and all free surface boundary conditions. Wave quantities are then expanded in power series in wave steepness ϵ, and written in Fourier series form as

$$\phi_{\mathrm{w}}=\sum_{n=1}^{\infty}\epsilon^{n-1}\sum_{m=-n}^{n}\phi^{(n,m)}(X_1,X_2,Y_1,Y_2,z,T_1,T_2) \times\exp(mi\psi(x,y,t)),\qquad m\neq0 \tag{19}$$

$$\eta_{\mathrm{w}}=\sum_{n=1}^{\infty}\epsilon^{n-1}\sum_{m=-n}^{n}\eta^{(n,m)}(X_1,X_2,Y_1,Y_2,z,T_1,T_2) \times\exp(mi\psi(x,y,t)),\qquad m\neq0 \tag{20}$$

with no zero-mode Fourier components as these are represented by $(\phi_{\mathrm{c}},\eta_{\mathrm{c}})$. Since we are dealing with real-valued physical variables, Fourier series coefficients are conjugate symmetric, i.e. $\phi^{(n,-m)}=\phi^{(n,m)*}$. The phase function ψ has derivatives

$$\nabla\psi=\boldsymbol{\kappa}=(k,l) \tag{21}$$

$$\psi_t=-\omega \tag{22}$$

and we further define the total wave number $\kappa \equiv |\boldsymbol{\kappa}|$. A corollary of the wave number definition gives

$$\nabla \times \boldsymbol{\kappa} = 0 \tag{23}$$

These definitions can be used to find an evolution equation for the local wave number vector

$$\boldsymbol{\kappa}_t = -\nabla\omega \tag{24}$$

The entire system is thus written in a set of ordered equations in terms of the short-wave velocity potential at the long-wave water level η_c. These may be solved at successively higher orders using the lower-order solutions as forcing.

For long-wave motion, the velocity potential is expanded nondimensionally and dispersively in the form

$$\Phi_c = \sum_{n=0}^{\infty} \Phi_c^{(n)}(Z+H)^n \tag{25}$$

as is standard for long waves (e.g. Wei et al., 1995) and is consistent with the assumed scaling. The long-wave surface elevation, η_c, is not expanded. In contrast to Eqs. (19) and (20), Eq. (25) is not an amplitude expansion and as such does not violate our earlier assumption that the current magnitude is $O(1)$.

The coefficients, $\Phi_c^{(n)}$, are set by using the long-wave scaled continuity condition together with the bottom boundary condition

$$\Phi_{cZZ} + \mu^2\nabla^2\Phi_c = 0, \qquad -H < Z < \eta_c \tag{26}$$

$$\Phi_{cZ} + \mu^2\nabla H \cdot \nabla\Phi_c = 0, \qquad z = -h \tag{27}$$

remembering $O(\mu) = O(\epsilon^2)$.

Omitting the details, which are standard (e.g. Wei et al., 1995), we arrive at

$$\Phi_c = \Phi_c^{(0)} - \mu^2(H+Z)\nabla H\nabla\Phi_c^{(0)} - \mu^2 \times \frac{(H+Z)^2}{2}\nabla^2\Phi_c^{(0)} + O(\mu^4) \tag{28}$$

and thus

$$\nabla\Phi_c = \nabla\Phi_c^{(0)} + O(\mu^2)$$

$$\Phi_{cZ} = -\mu^2\nabla\cdot[(Z+H)\nabla\Phi_c^{(0)}] + O(\mu^4)$$

$$\Phi_{cXZ} = O(\mu^2)$$

$$\Phi_{cZZ} = -\mu^2\nabla\cdot\Phi_c^{(0)} + O(\mu^4) \tag{29}$$

confirming the earlier assumed results of Eq. (10).

Again, after transforming back to dimensional quantities, the leading order long-wave velocity potential, $\phi_c^{(0)}$, will simply be written as ϕ_c.

At each perturbation level, the short-wave system takes the form of a set of equations

$$\nabla^2\phi^{(n,m)} + \phi_{zz}^{(n,m)} = R^{(n,m)}, \qquad -h \le z \le \eta_c \tag{30}$$

$$\phi_z^{(n,m)} = F^{(n,m)}, \qquad z = -h \tag{31}$$

$$\Gamma_w\phi^{(n,m)} = G^{(n,m)}, \qquad z = \eta_c \tag{32}$$

where forcing to the right-hand sides is provided by solutions from lower-order $n-1$, $n-2$, etc.

To solve the system at each order, it is first necessary to solve the forced and free flow fields defined by Eqs. (30) and (31). The resulting velocity field is then substituted into Eq. (32) to arrive at dispersion relations, evolution equations and such.

It is possible to combine these two steps to yield directly solvability conditions (e.g. Chu and Mei, 1970; Liu and Dingemans, 1989); however, we feel that it is instructive to keep the two processes separate, and will proceed in this way.

The solution to Eqs. (30) and (31) is (Chu and Mei, 1970)

$$\phi^{(n,m)} = A^{(n,m)}\cosh mQ + \frac{1}{m\kappa}F^{(n,m)}\sinh mQ + \frac{1}{m\kappa^2}\left\{\sinh mQ\int_0^Q R^{(n,m)}\cosh mQ'\,dQ' - \cosh mQ\int_0^Q R^{(n,m)}\sinh mQ'\,dQ'\right\} \tag{33}$$

where $Q \equiv \kappa(h+z)$.

This is then substituted into the free surface boundary condition Eq. (32) which, depending on the level of approximation and Fourier mode, will either define the frequency–wave number relationship, fix a previously free coefficient or define an evolution equation.

3.1. Order (ϵ)

For $m=1$, forcing functions are

$$R^{(1,1)} = F^{(1,1)} = G^{(1,1)} = 0 \tag{34}$$

From Eq. (33), this yields

$$\begin{aligned}\phi^{(1,1)} &= A^{(1,1)}\cosh Q \\ &= \frac{-ig}{2\sigma} A \frac{\cosh Q}{\cosh q} \\ &= AB\cosh Q\end{aligned} \tag{35}$$

where $q \equiv \kappa(h+\eta_c)$. The redefinition of the free coefficient $A^{(1,1)}$ is not strictly necessary, but is performed since A now represents the local wave amplitude, and with foreknowledge that it simplifies somewhat the rest of the derivation.

Substituting Eq. (35) into Eq. (32) yields the well-known linear dispersion relation for plane waves on a current

$$\sigma^2 = g\kappa\tanh(q) \tag{36}$$

where the intrinsic frequency $\sigma \equiv \omega - \boldsymbol{\kappa}\cdot\nabla\phi_c$.

3.2. Order (ϵ^2)

At $O(\epsilon^2)$, $m=1$ yields forcing

$$R^{(2,1)} = -2[\phi^{(1,1)}_{X_1x} + \phi^{(1,1)}_{Y_1y}]$$

$$F^{(2,1)} = 0$$

$$\begin{aligned}G^{(2,1)} = -2\Big\{ &\phi^{(1,1)}_{tT_1} + [\phi_{cx}(\phi^{(1,1)}_{xT_1} + \phi^{(1,1)}_{X_1t}) + \phi_{cy}(\phi^{(1,1)}_{yT_1} \\ &+ \phi^{(1,1)}_{Y_1t})] + \phi_{cx}\phi_{cx}\phi^{(1,1)}_{xX_1} + \phi_{cx}\phi_{cx}(\phi^{(1,1)}_{yX_1} \\ &+ \phi^{(1,1)}_{xY_1}) + \phi_{cy}\phi_{cy}\phi^{(1,1)}_{yY_1}\Big\}\end{aligned} \tag{37}$$

As defined, slow derivatives do not in general commute, e.g. $\phi_{xX_2} \neq \phi_{X_2}x$. However, in this particular case, we have made use of the fact that $\phi_{xX_1} = \phi_{X_1}x$ to simplify the equations somewhat.

From Eq. (33), the second-order velocity potential becomes

$$\phi^{(2,1)} = A^{(2,1)}\cosh Q - i\frac{B\nabla_1 A\cdot\boldsymbol{\kappa}}{\kappa^2} Q\sinh Q \tag{38}$$

The second term is the particular solution, while the first term is the homogeneous solution to the continuity equation, as was found in Eq. (35). This homogeneous term could present complications if not dealt with, as it is a free parameter. Chu and Mei (1970) specified this term based on deep water solutions, while Liu and Dingemans (1989) incorporated it in a redefinition of the dependent variable, A. For the present case, this last technique is functionally the same as specifying $A^{(2,1)}=0$ and thus we will specify all $A^{(n,1)}=0$, $n\neq 1$.

Substituting Eq. (38) into Eq. (32) gives an evolution equation

$$A_{T_1} + (\mathbf{C}_g + \nabla\phi_c)\nabla_1 A = 0 \tag{39}$$

which describes the transport of wave energy at the local group velocity where

$$\mathbf{C}_g \equiv C_g \frac{\boldsymbol{\kappa}}{\kappa} \tag{40}$$

and

$$C_g \equiv \frac{\sigma}{2\kappa}\left(1 + \frac{2q}{\sinh 2q}\right) \tag{41}$$

At $m=2$, the forcing is

$$R^{(2,2)} = 0$$

$$F^{(2,2)} = 0$$

$$\begin{aligned}G^{(2,2)} = &-D(\nabla^{(3)}\phi^{(1,1)}\cdot\nabla^{(3)}\phi^{(1,1)}) \\ &+ \frac{1}{g}(\phi^{(1,1)}_t + \nabla\phi_c\cdot\nabla\phi^{(1,1)})\Gamma\phi^{(1,1)}_z\end{aligned} \tag{42}$$

giving a velocity potential

$$\phi^{(2,2)} = A^{(2,2)}\cosh 2Q \tag{43}$$

Inserting this into Eq. (42) yields the well-known second harmonic for a second-order Stokes plane wave on a current

$$\begin{aligned}\phi^{(2,2)} &= -i\frac{3}{16}\sigma A^2 \frac{\cosh 2Q}{\sinh^4 q} \\ &= B\kappa A^2 \frac{3}{8}\frac{\cosh 2Q}{\sinh^3 q}.\end{aligned} \tag{44}$$

3.3. Order (ϵ^3)

By a basic assumption of the derivation, all low frequency ($m=0$) motion is encapsulated in (ϕ_c, η_c) and thus the time variations of these quantities include forcing from all perturbation levels up to $O(\epsilon^3)$. Thus, only one low frequency evolution equation is needed for all perturbation levels if we use Eq. (6). However, we shall instead develop separate equations for the evolution of free surface elevation and velocity, as this is standard practice for nearshore circulation models.

The conservation of mass Eq. (4) yields, for low frequency motion,

$$\epsilon^2[\eta_{ct} + \nabla\cdot((h+\eta)\nabla\phi_c)] + \epsilon^3[\nabla\cdot\mathbf{Q}] = 0, \quad z = \eta_c \tag{45}$$

where $\mathbf{Q}$ represents short-wave volume flux, given by

$$\mathbf{Q} = \frac{g}{2}\frac{|A^2|}{\mathrm{c}}(\cos\alpha, \sin\alpha) \tag{46}$$

The Bernoulli equation for conservation of energy gives

$$\epsilon^2\left[\phi_{ct} + g\eta + \frac{1}{2}(\phi_{cx}^2 + \phi_{cy}^2)\right] + \epsilon^3[\mathrm{SWF_{tmp}}] = 0, \quad z = \eta_c \tag{47}$$

where the short-wave forcing is left in schematic form.

We have deliberately been vague about the form of these equations for several reasons. Firstly, we intend to use them in the surf zone, where our theory is formally invalid for even moderate wave nonlinearity. Thus, semi-empirical modifications to the forcing terms may be necessary. The second reason for this lack of detail is that Eq. (47) by definition cannot model vertical vorticity in the current. Since vorticity is an integral part of nearshore currents induced by wave breaking (see, e.g. Peregrine, 1998), modifications must be made to our theory to allow for this.

In common with our goal of providing forcing for nearshore circulation models, instead of Eq. (47), we will use

$$\tilde{\mathbf{U}}_t + g\nabla\eta + (\tilde{\mathbf{U}}\cdot\nabla)\tilde{\mathbf{U}} + \mathrm{RS} = 0 \tag{48}$$

which is simply the nonlinear shallow water equations including forcing from short-wave radiation stresses. The mass transport velocity $\tilde{\mathbf{U}} \equiv \mathbf{U} + \mathbf{Q}/(h+\eta)$ is used, as it makes computations considerably simpler. This approach was taken by Longuet-Higgins (1970a,b) and is almost universally used in whole or in part by existing wave-driven nearshore circulation models. This also simplifies the conservation of mass equation, which becomes

$$\eta_t + \nabla\cdot[(h+\eta)\tilde{\mathbf{U}}] = 0. \tag{49}$$

For nonbreaking waves, the radiation stress forcing takes the form

$$\mathrm{RS} = \frac{1}{h+\eta_c}\Big([S_m\cos^2\alpha + S_p]_x + [S_m\sin\alpha\cos\alpha]_y, \; [S_m\sin^2\alpha + S_p]_y + [S_m\sin\alpha\cos\alpha]_x\Big) \tag{50}$$

where α is the angle between the wave direction and the positive x-axis, and

$$S_m = \frac{1}{4}g|A^2|(1+G) \tag{51}$$

$$S_p = \frac{1}{4}g|A^2|G \tag{52}$$

where

$$G \equiv \frac{2q}{\sinh 2q}. \tag{53}$$

The angle of incidence, α, is defined by

$$\alpha = \arctan\left(\frac{l}{k}\right) \tag{54}$$

keeping track of the quadrant to ensure that the full circle can be covered.

In the surf zone, volume flux and radiation stress relations change significantly, partially due to very strong nonlinear interactions and partially because of roller effects. Numerous authors have studied these changes (e.g. Svendsen, 1984). We will not include these changes in our present model, but they may easily be added by including empirical modifications to the existing values.

For $n=3$, $m=1$, the forcing becomes

$$R^{(3,1)} = -2[\phi_{X_1x}^{(2,1)} + \phi_{Y_1y}^{(2,1)}] - [\phi_{xX_2}^{(1,1)} + \phi_{X_2x}^{(1,1)} + \phi_{yY_2}^{(1,1)} + \phi_{Y_2y}^{(1,1)}]$$

$$F^{(3,1)} = -\nabla_2 h \nabla \phi^{(1,1)}$$

$$\begin{aligned}
G^{(3,1)} = & -2[\phi_{tT_1}^{(2,1)} + \phi_{cx}(\phi_{X_1 t}^{(2,1)} + \phi_{xT_1}^{(2,1)}) + \phi_{cy}(\phi_{y_1 t}^{(2,1)} \\
& + \phi_{yT_1}^{(2,1)}) + \phi_{cx}(\phi_{cx}\phi_{xX_1}^{(2,1)} + \phi_{cy}\phi_{X_1 y}^{(2,1)}) \\
& + \phi_{cy}(\phi_{cx}\phi_{xY_1}^{(2,1)} + \phi_{cy}\phi_{yY_1}^{(2,1)})] - [\phi_{T_1 T_1}^{(1,1)} \\
& + 2(\phi_{cx}\phi_{X_1 T_1}^{(1,1)} + \phi_{cy}\phi_{Y_1 T_1}^{(1,1)}) + \phi_{cx}(\phi_c x \phi_{X_1 X_1}^{(1,1)} \\
& + \phi_{cy}\phi_{Y_1 Y_1}^{(1,1)})] - [\phi_{tT_2}^{(1,1)} + \phi_{T_2 t}^{(1,1)} + 2\phi_{cx}(\phi_{X_2 t}^{(1,1)} \\
& + \phi_{xT_2}^{(1,1)}) + 2\phi_{cy}(\phi_{Y_2 t}^{(1,1)} + \phi_{yT_2}^{(1,1)}) + \phi_{cx}^2(\phi_{xX_2}^{(1,1)} \\
& + \phi_{X_2 x}^{(1,1)}) + 2\phi_{cx}\phi_{cy}(\phi_{X_2 y}^{(1,1)} + \phi_{xY_2}^{(1,1)}) \\
& + \phi_{cy}^2(\phi_{yY_2}^{(1,1)} + \phi_{Y_2 y}^{(1,1)})] - [2\phi_{cz}^{(2)}\phi_{zt}^{(1,1)} \\
& + 2\nabla\phi_{ct} \cdot \nabla\phi^{(1,1)} + \phi_{cx}\nabla\phi_{cx} \cdot \nabla\phi^{(1,1)} \\
& + \phi_x^{(1,1)}\nabla\phi_c \cdot \nabla\phi_{cx} + \phi_{cy}\nabla\phi_{cy} \cdot \nabla\phi^{(1,1)} \\
& + \phi_y^{(1,1)}\nabla\phi_c \cdot \nabla\phi_{cy} + 2\phi_{cz}^{(2)}\nabla\phi_c \cdot \nabla\phi_z^{(1,1)}] \\
& + \phi_{czz}^{(2)} D\phi^{(1,1)} + \frac{1}{g}\Bigg[-\frac{1}{g}\phi_t^{(1,1)}\phi_{zt}^{(1,1)} \\
& + \frac{1}{2}(\nabla^{(3)}\phi^{(1,1)} \cdot \nabla^{(3)}\phi^{(1,1)})\Bigg]\Gamma\phi_z^{(1,1)} \\
& - \nabla^{(3)}\phi^{(1,1)} \cdot \nabla^{(3)}(\nabla^{(3)}\phi^{(1,1)} \cdot \nabla^{(3)}\phi^{(1,1)}) \\
& - \frac{1}{2g^2}[\phi_t^{(1,1)} + \nabla\phi_c \cdot \nabla\phi^{(1,1)}]^2 \Gamma\phi_{zz}^{(1,1)} \\
& + \frac{2}{g}[\phi_t^{(1,1)} + \nabla\phi_c \cdot \nabla\phi^{(1,1)}] \\
& \times (\nabla^{(3)}\phi_z^{(1,1)} \cdot \nabla^{(3)}\phi^{(1,1)}) \qquad (55)
\end{aligned}$$

where it is understood that, for the nonlinear terms, we are only interested in the first harmonic component.

The first harmonic velocity potential becomes

$$\begin{aligned}
\phi^{(3,1)} = & A^{(3,1)}\cosh Q - i\frac{B\nabla_2 A \cdot \boldsymbol{\kappa}}{\kappa^2} Q\sinh Q - iAB \\
& \times \Bigg[\frac{\nabla_2 h \cdot \boldsymbol{\kappa}}{\kappa}\sinh Q + \left(\frac{\nabla_2 \cdot \boldsymbol{\kappa}}{2\kappa^2} - \frac{\boldsymbol{\kappa} \cdot \nabla_2 \sigma}{\kappa^2 \sigma}\right) \\
& \times Q\sinh Q + \frac{1}{2}\frac{\nabla_2 \kappa \cdot \boldsymbol{\kappa}}{\kappa^3}(Q^2\cosh Q - Q\sinh Q) \\
& + \frac{\boldsymbol{\kappa} \cdot \nabla_2 h}{\kappa}(Q\cosh Q - \sinh Q) \\
& - \frac{\boldsymbol{\kappa} \cdot \nabla_2 q}{\kappa^2}\tanh q Q\sinh Q\Bigg] \qquad (56)
\end{aligned}$$

After a large amount of algebra, repeatedly invoking Eq. (39) to eliminate A_{tt}, etc., terms, and translating back from multiple scales to normal dimensions including all orders, the end result of Eq. (55) is an equation for the evolution of the wave envelope in space and time

$$\begin{aligned}
& 2A_t + 2(\mathbf{C}_g + \mathbf{U}) \cdot \nabla A + \left[\sigma\nabla \cdot \left(\frac{\mathbf{C}_g + \mathbf{U}}{\sigma}\right) - \frac{1}{\sigma}\sigma_t\right]A \\
& - i\frac{C_g}{\kappa}\nabla^2 A + i\left(\frac{C_g}{\kappa} - \sigma_{\kappa\kappa}\right) \\
& \times \left(\frac{A_{xx}k^2 + 2A_{xy}kl + A_{yy}l^2}{\kappa^2}\right) + i\sigma\kappa^2\beta|A^2|A = 0 \qquad (57)
\end{aligned}$$

where we write $\mathbf{U} \equiv \nabla\phi_c$, and

$$\sigma_{\kappa\kappa} = \frac{c}{\kappa}[q\coth q - n^2 - 2n\tanh q] \qquad (58)$$

$$\beta = \frac{\cosh 4q + 8 - 2\tanh^2 q}{8\sinh^4 q} \qquad (59)$$

This system of equations will be referred to as method 1.

When combined with Eqs. (24), (48) and (49), this gives a system capable of computing combined wave–current motion in the nearshore for weakly nonlinear, narrowbanded waves varying mildly in amplitude and direction from a given wave number. This wave number vector field is not necessarily shore-normal: a simple example would be an underlying vector field on a plane beach computed from Snell's law. More complex examples are of course possible, although, as will be seen very soon, there do exist environments where underlying refraction fields cannot be defined.

It is helpful to think of method 1 as the conservation of wave action equations with additional terms to account for narrow angle diffraction and nonlinear dispersion. This relaxes somewhat the long-crested assumption implicit in conservation of wave action and allows wave evolution to be computed in areas where transformation is more rapid than before.

3.4. Modified equations—regularised underlying bathymetry

The system-denoted method 1 will work well for a variety of situations in the nearshore. However, there are several relatively common conditions in which its basic assumptions are violated. For these situations, answers may still come out of the model, but they cannot be trusted.

The classical example of why modifications are needed occurs when topographic or current focusing causes caustics in the underlying wave number field. The method 1 equations are fundamentally unable to examine this situation, as a well-behaved wave number vector field does not exist. For topographic focusing, the cause is often a submerged shoal (e.g. Berkhoff et al., 1982), which can be all too common when modeling real-world situations. A somewhat less common situation (mostly found at rip currents and inlets) occurs when currents focus wave rays. In both cases, it becomes impossible to satisfy both the dispersion relation (36) and the requirement that the wave number vector field is irrotational (Eq. (23)). For any given topography, underlying wave number vector fields may be defined which satisfy one of the two conditions, and answers would result from the model as defined in Eq. (57). However, the answers would be wrong, as the basic assumptions of derivation have been violated.

Since we wish to study these more difficult conditions, in such cases, it becomes preferable to modify the equation for evolving wave amplitude. This is done by first assuming conditions in which the underlying wave number vector field can never have caustics: the actual conditions to be studied are then treated as a perturbation about this base condition. For the general situation, some small accuracy may be lost, but this approximation allows us to study situations which previously were not possible.

Specifically, we assume

$$h = \bar{h} + \epsilon^2 \hat{h}, \quad \eta_c = \bar{\eta}_c + \epsilon^2 \hat{\eta}_c, \quad \mathbf{U} = \bar{\mathbf{U}} + \epsilon^2 \hat{\mathbf{U}} \tag{60}$$

The simplest situation which guarantees the requisite wave number vector field is a longshore uniform, but not necessarily planar, beach with no currents. More complex underlying geometries are possible; as long as a suitable wave number field can be guaranteed at all times, they will work well. However, because the wave number field must be well-behaved at all times, for many situations without prior knowledge, it may be necessary to assume that $\bar{\eta}_c = 0$, $\bar{\mathbf{U}} = 0$. These assumptions are generally similar to those of Lozano and Liu (1980), who also used a regularised bathymetry to remove singularities in the underlying wave number field of a parabolic model with no current.

Because the assumed scaling of the perturbation is $O(\epsilon^2)$, we only need to consider the leading order correction to Eq. (57): for a stronger correction of $O(\epsilon)$, additional terms would result.

These leading order corrections result from the fact that the linear dispersion relationship (36) is not analytically satisfied when the underlying quantities ($\bar{\kappa}$, $\bar{\eta}_c$, $\bar{\mathbf{U}}$) and the actual water depth, h, are used. The resulting error is $O(\epsilon^3)$ and appears in the evolution equation.

After some algebra, the modified evolution equation becomes

$$\begin{aligned} &2A_t + 2(\bar{\mathbf{C}}_g + \bar{\mathbf{U}}) \cdot \nabla A + \left[\bar{\sigma} \nabla \cdot \left(\frac{\bar{\mathbf{C}}_g + \bar{\mathbf{U}}}{\bar{\sigma}}\right) - \frac{1}{\bar{\sigma}} \bar{\sigma}_t\right] A \\ &\quad - 2iA(\bar{C}_g(\kappa - \bar{\kappa}) + \hat{\kappa} \cdot \bar{\mathbf{U}}) - i \frac{\bar{C}_g}{\bar{\kappa}} \nabla^2 A \\ &\quad + i\left(\frac{\bar{C}_g}{\bar{\kappa}} - \bar{\sigma}_{\bar{\kappa}\bar{\kappa}}\right)\left(\frac{A_{xx}\bar{k}^2 + 2A_{xy}\bar{k}\bar{l} + A_{yy}\bar{l}^2}{\bar{\kappa}^2}\right) \\ &\quad + i\bar{\sigma}\bar{\kappa}^2 \beta |A^2| A = 0 \end{aligned} \tag{61}$$

where $\hat{\kappa} = (\kappa - \bar{\kappa})\bar{\boldsymbol{\kappa}}/\bar{\kappa}$

Using the relationships $C_g = \bar{C}_g + O(\epsilon^2)$, $\tilde{\mathbf{U}} = \mathbf{U} + \epsilon^2 \mathbf{Q}/Ch + O(\epsilon^3)$, etc., this may be rewritten into an asymptotically identical form

$$\begin{aligned} &2A_t + 2(\mathbf{C}_g + \tilde{\mathbf{U}}) \cdot \nabla A + \left[\sigma \nabla \cdot \left(\frac{\mathbf{C}_g + \tilde{\mathbf{U}}}{\sigma}\right) - \frac{1}{\sigma} \sigma_t\right] A \\ &\quad - 2iA(C_g(\kappa - \bar{\kappa}) + \hat{\kappa} \cdot \tilde{\mathbf{U}}) - i \frac{C_g}{\kappa} \nabla^2 A \\ &\quad + i\left(\frac{C_g}{\kappa} - \sigma_{\kappa\kappa}\right)\left(\frac{A_{xx}k^2 + 2A_{xy}kl + A_{yy}l^2}{\kappa^2}\right) \\ &\quad + i\sigma\kappa^2 \beta |A^2| A = 0 \end{aligned} \tag{62}$$

This form is preferred as it preserves better shoaling and transport over the real bathymetry and will be referred to as method 2. Both the long-wave and short-wave equations now use the mass transport velocity rather than the Eulerian velocity.

For Eq. (61), the wave number evolution equation is

$$\bar{\kappa}_t = -\nabla \bar{\omega} \tag{63}$$

where $\bar{\omega}$ is calculated using regularised quantities. Thus, if $\bar{\mathbf{U}}=\bar{\eta}_c=0$, the initial underlying wave number field satisfies linear dispersion (36) and irrotationality (23) and the wave frequency never changes at the boundary, then from Eq. (63), the underlying wave number field never varies and thus will always be irrotational and satisfy the dispersion relationship.

3.4.1. Modified wave nonlinearity in shallow water

Stokes-type expansions for water waves diverge for moderate wave heights in shallow water. We include a semi-empirical modification to the cubic nonlinear term, first used by Kirby and Dalrymple (1986), in order to avoid the singularity. In this modification, the term $i\sigma\kappa^2\beta|A^2|A$ in Eq. (57) or Eq. (61) is replaced by

$$i\sigma A\left[(1+f_1\kappa^2|A|^2\beta)\frac{\tanh(\kappa h+f_2\kappa|A|)}{\tanh\kappa h}-1\right] \tag{64}$$

where

$$f_1=\tanh^5(\kappa h) \tag{65}$$

$$f_2=[\kappa h/\sinh(\kappa h)]^4 \tag{66}$$

This empirically interpolates phase speeds between Stokes theory in deep water and solitary wave theory in shallow water, giving a reasonable approximation of nonlinear phase speed in all water depths. Kirby and Dalrymple (1986) have demonstrated that this modification to the model effectively eliminates the singularity of Stokes theory, allowing the model to be used in shallow water and the surf zone, without damaging nonlinear properties in intermediate water depths.

4. Numerical approach

All computations here use the modified equations, as we will examine some complex transformations. The numerical approach uses standard finite differences. All convective terms are treated using second-order upwinding, while other spatial derivatives use second-order central differences. Walls form the onshore and offshore boundaries, while lateral boundaries may be either periodic or reflective. For the reflective case, symmetry considerations are used to modify finite difference formulae in the vicinity of the wall. Time differencing uses a second-order Crank–Nicolson implicit scheme. The simple shallow water scheme (48) is extended to include bottom friction and subgrid mixing as

$$\tilde{\mathbf{U}}_t+g\nabla\eta+(\tilde{\mathbf{U}}\cdot\nabla)\tilde{\mathbf{U}}+\mathrm{RS}+F_{\mathrm{NL}}+F_{\mathrm{L}}+\mathrm{SG}=0 \tag{67}$$

Bottom friction includes both linear and nonlinear components, defined by

$$F_{\mathrm{L}}=C_{\mathrm{L}}\sqrt{g/(h+\eta+\epsilon)}\tilde{\mathbf{U}} \tag{68}$$

and

$$F_{\mathrm{NL}}=\frac{f_{\mathrm{NL}}}{(h+\eta+\epsilon)}\tilde{\mathbf{U}}|\tilde{\mathbf{U}}| \tag{69}$$

where f_{NL} and C_{L} are dimensionless constants and ϵ here is a small positive quantity that ensures denominators can never reach zero. Subgrid mixing SG uses Smagorinsky-type dissipation which depends on gradients in the mean flow (e.g. Chen et al., 1999).

Breaking here uses a simple depth-limited scheme that imposed $2|A|\leq 0.8$ at all time steps. Subsequent papers will use more complex breaking dissipation, but for the phenomena examined here, the simple scheme worked well.

The simple shallow water scheme used here requires a minimum depth at the shoreline to remain stable, but in the future, a better shoreline condition is envisaged. A wide linear damping layer is placed offshore to absorb reflected long waves during unsteady tests.

5. Test case: wave focusing by an elliptical shoal

The experiments of Berkhoff et al. (1982, BBR) have often been used to evaluate wave models. These experiments feature strong wave focusing behind a shoal situated on a plane beach, with resulting strong diffraction. As such, it provides a good initial test for the wave transformation portion of the model. An added bonus is that numerous

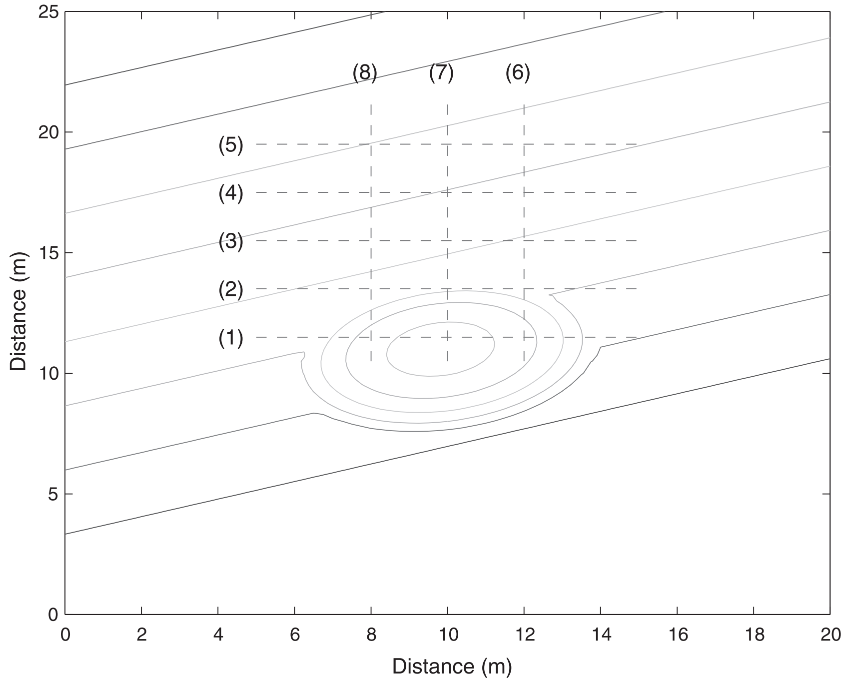

Fig. 1. Contours of bathymetry on BBR shoal, showing measurement transects.

investigators have studied this shoal, and their results may be compared.

Fig. 1 shows bathymetric contours for the experimental setup. After a coordinate transformation

$$x' = (x - 10.5\ \text{m})\cos(20°) - (y - 10\ \text{m})\sin(20°)$$

$$y' = (x - 10.5\ \text{m})\sin(20°) + (y - 10\ \text{m})\cos(20°) \tag{70}$$

the slope may be described by

$$h_S = \begin{cases} 0.45\ \text{m} & x' < -5.82\ \text{m} \\ 0.45 - 0.02(5.82 + x')\ \text{m} & x' > -5.82\ \text{m} \end{cases} \tag{71}$$

The shoal boundary is given by

$$\left(\frac{x'}{3\ \text{m}}\right)^2 + \left(\frac{y'}{4\ \text{m}}\right)^2 = 1 \tag{72}$$

Inside the shoal, the depth becomes

$$h = h_S - (0.5\ \text{m})\left[1 - \left(\frac{x'}{3.75\ \text{m}}\right)^2 - \left(\frac{y'}{5\ \text{m}}\right)^2\right]^{1/2} + 0.3\ \text{m} \tag{73}$$

Measurements of wave height were taken by BBR along eight transects: five perpendicular to and three parallel to the main direction of wave propagation. Fig. 1 shows the transect locations. More details may be found in Berkhoff et al. (1982).

This topography leads to strong focusing of wave rays, with caustics occurring behind the shoal. Because of this, method 1 may not be used on this topography, as an underlying refraction solution does not exist. However, method 2 is well suited to such a computation. The underlying bathymetry was assumed to be a longshore uniform beach, whose depth was chosen to be the average over the longshore domain. A computational grid size of $\Delta x = \Delta y = 0.25$ m was used with a time step of $\Delta t = 0.025$ s. Lateral boundaries used a reflective condition, which is considerably different than the physical experiment, but as boundaries were far away from the area of interest, this was not a concern.

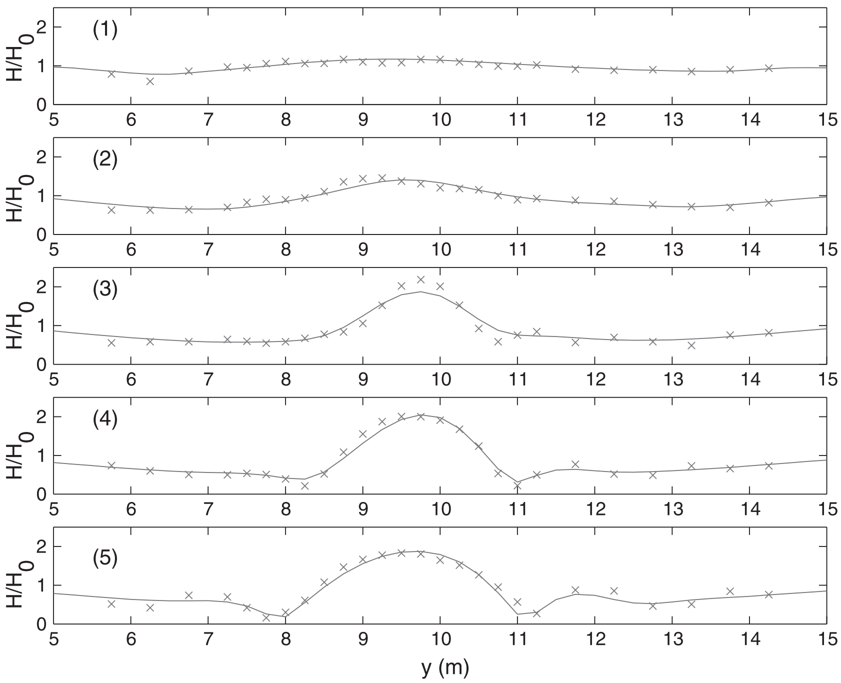

Fig. 2. Computed (–) and measured (×) wave heights at transects 1–5 on BBR shoal.

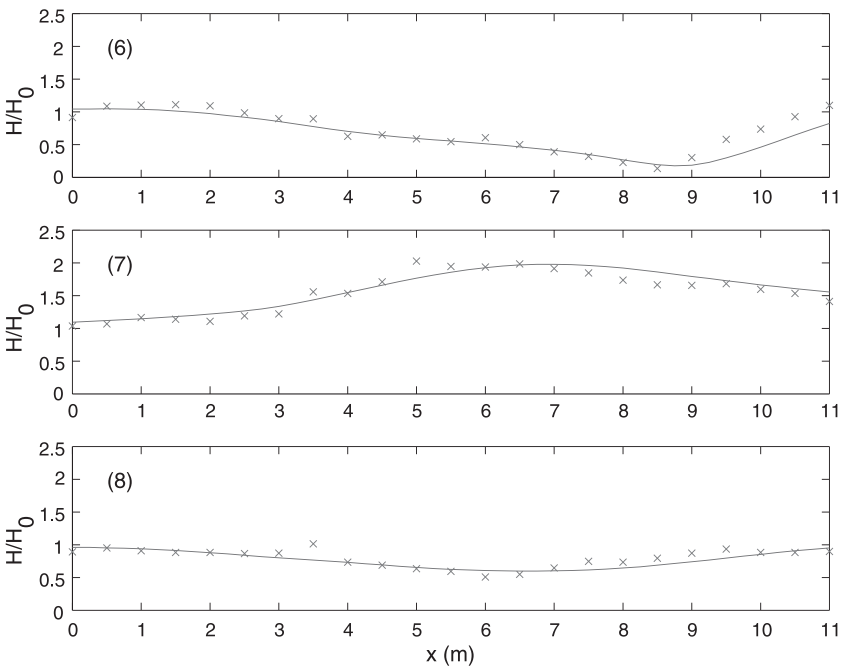

Fig. 3. Computed (–) and measured (×) wave heights at transects 6–8 on BBR shoal.

Formally, the physical wave height in computations is not just $H=2|A|$ but includes higher-order corrections. However, because of the semi-empirical modifications to nonlinear dispersion, with unknown effects on surface profiles, we use this simpler representation. For some situations, this approximation would be unacceptably crude; however, for the present case, reasonable results may still be obtained.

Figs. 2 and 3 show computed and measured wave heights along the transects. In general, agreement is quite good. Both the trend and the magnitude of the refraction and diffraction caused by the shoal are well represented. The present results look very similar to those computed using the narrow angle parabolic model given in Kirby and Dalrymple (1986). This is not surprising as, with the further assumptions of time invariance, weak diffraction in the direction of propagation and negligible current, the two models are equivalent. Since none of these effects are likely to be highly significant in this case, the results are very similar.

Although the present results are good, it is possible to achieve slightly greater accuracy by using full time-domain systems such as Boussinesq models (e.g. Wei et al., 1995). This is because these models do not assume an underlying form for the wave and thus can represent better the strong nonlinear diffraction. Still, Boussinesq models are computationally an order of magnitude slower than the present model and thus cannot be easily used for long-time scales in field situations. Wide-angle parabolic models can also produce slightly better results in this case (e.g. Kirby, 1986), as their treatment of diffraction is more accurate. This improvement in accuracy is mainly seen in the side lobes of longshore transects 4–5, where the wide-angle approximation allows for more accurate diffraction far from the mean wave direction. Overall, however, agreement is quite good using the present model and gives confidence that accurate refraction/diffraction/shoaling results can be obtained in situations for which no direct confirmation is available.

6. Edge wave generation on longshore nonuniform beaches

Edge waves have been measured in the nearshore on numerous equations (Oltman-Shay and Guza, 1987; Özkan-Haller et al., 2001), usually with amplitudes of O(centimetres) and wavelengths of O(hundreds of metres). However, the processes leading to their generation are still not entirely clear. Theories range greatly from predicting edge waves at twice incident wave periods (Guza and Davis, 1974; only suitable for waves with scales of beach cusps) to edge waves associated with short-wave frequency–wave number pairs satisfying the edge wave dispersion relationship (Lippmann et al., 1997). There exist numerous other theories and none have been accepted as definitive. In fact, it is likely that different generation mechanisms may be important in different situations.

On beaches that are not too steep, edge waves can be approximated using the shallow water equations. On a planar beach of slope m and given alongshore wave number k, a number of discrete modes exist with frequencies

$$\omega^2 = gmk(2n+1) \tag{74}$$

where ω is the frequency, g is downwards gravitational acceleration and n is the integer mode number representing the number of zero crossings of the free surface elevation in the cross-shore. The free surface elevation of a linear progressive edge wave is then given by

$$\eta = a_n L_n(2kx)\exp(-kx)\cos(kx-\omega t) \tag{75}$$

where a_n is the shoreline amplitude and L_n is the Laguerre polynomial of order n.

Standing edge waves may of course be formed by superimposing two oppositely travelling waves of equal amplitude, frequency and mode number to get

$$\eta = a_{ns} L_n(2kx)\exp(-kx)\cos(kx)\cos(\omega t) \tag{76}$$

Using the system developed here, we examine an alternative method of edge wave generation, namely, from the interaction of wave groups with longshore bathymetric nonuniformities. This gives a viable explanation for edge wave generation in a number of common situations.

Conceptually, this is easiest to explain for periodic longshore topographies and shore-normal, periodic wave groups. As waves approach the shoreline, refraction and longshore bathymetric perturbations will create periodic longshore variations in wave height, with corresponding variations in breaking strength. When forcing varies temporally with wave groups, we then see time-periodic forcing (with the period of the wave groups) combined with space-periodic forcing (on the length of the longshore periodicities). If the period and wavelength satisfy the edge wave dispersion relationship, resonant growth will result, while other wavelength-group period combinations will give smaller amplitude results.

The basic concept is similar to that of Foda and Mei (1981), who imposed longshore-periodic variations in wave height on time-varying wave amplitudes, propagated waves onto a plane beach and found that resonances could occur. However, they provided no source for their variations in wave height, which continued through the surf zone contrary to most accepted practices.

In contrast, linking variations in wave height and breaking to longshore depth variations provide a solid physical basis between incoming wave groups and edge waves. On many, if not most, shorelines, there are appreciable longshore bathymetric variations with length scales of hundreds of metres. With this background, it becomes difficult to see how edge waves could not be generated by unsteady wave forcing.

6.1. Shore-normal, bichromatic wave groups

To demonstrate this generation mechanism, we send shoreward bichromatic wave groups over a planar beach of slope 0.03 with a small cosine variation in the longshore, with amplitude 0.01 m and wave number $k = 2\pi/500\ \mathrm{m}^{-1}$. Thus, the bathymetry is

$$h = 18 - 0.03x + 0.01\cos(ky) \tag{77}$$

where the computational domain extends offshore to a depth of 18 m. A sponge layer is used offshore to prevent re-reflection of long waves, and a minimum depth of 0.15 m is used at the shoreline. We will only consider mode zero edge waves here, but other modes will also be excited if the wave number–frequency relationship is satisfied.

Wave groups are created using bichromatic forcing, with amplitudes $a_1 = 2a_2$, which gives an overall height $H_{\mathrm{RMS}} = 2(a_1^2 + a_2^2)^{1/2}$. With frequencies f_1 and f_2, this gives a time-periodic wave forcing at frequency $f_1 - f_2$. When this is near any edge wave period, a strong response is expected. No forcing in these tests is anywhere near basin resonances.

For simplicity and consistency, we will define edge wave amplitudes by projecting water surfaces onto free edge wave modes so that any instantaneous water surface is seen as the sum of normal modes. This definition was chosen after some consideration, as it allows the changing shape of the response at the group frequency to be easily defined for both resonant and nonresonant conditions. An alternative would be to consider the total response at the group frequency as a new, forced mode (e.g. Henderson and Bowen, submitted for publication). We have chosen not to do this as near resonance one mode dominates. Away from resonance, amplitudes of the different normal modes are more comparable, but they are all small and contribute little to the overall climate.

Fig. 4 shows equilibrium mode zero edge wave amplitudes for a 10-s peak period and wave heights at 18-m depth of $H_{\mathrm{RMS}} = 0.75$ and 1.0 m and using friction coefficients $f_{\mathrm{NL}} = 0.005$ and $C_{\mathrm{L}} = 0.0002$. A strong resonance peak is visible near $f = 0.0103$ Hz, which corresponds fairly well to the edge wave frequency of $f = 0.0097$ Hz on the unperturbed bathymetry. Differences are believed to be due in large part to the presence of the minimum depth which, in conjunction with setup, means that actual normal modes will be somewhat different. This point will be expanded on later.

Of particular note is that at the resonance peak, edge wave amplitudes are much larger than the amplitude of the bathymetric perturbation. Thus, even the small perturbation used with amplitude 1 cm is sufficient to generate edge waves of O(10 cm), which are relatively large.

Results are quite sensitive to bottom friction. Fig. 5 shows results using doubled friction coefficients. Peak amplitudes are decreased considerably, but away from resonance, results are still comparable. As field bottom friction may not be known in advance, it may thus prove difficult to obtain quantitative matches with field data.

One more subtle concern is the definition of edge waves. The presence of the minimum depth, longshore variations and setup combine to modify edge wave mode shapes and frequencies from the no setup, planar bed case (Eqs. (74) and (75)). These mode s0hapes on perturbed bathymetries vary enough from the simple cases that estimates of edge wave amplitudes will vary considerably. All previous

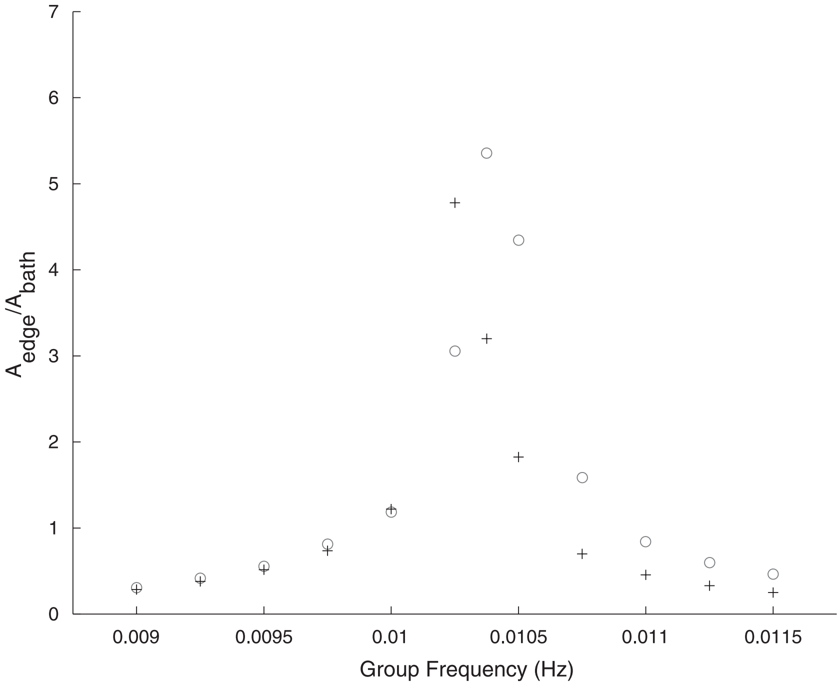

Fig. 4. Edge wave amplitudes over a plane beach with longshore cosine variation and bichromatic forcing. $T_p = 10$ s; $m = 0.03$; $k = 2\pi/500$ m^{-1}; $f_{NL} = 0.005$; $C_L = 0.0002$. ○: $H_{RMS} = 1.0$ m; +: $H_{RMS} = 0.75$ m.

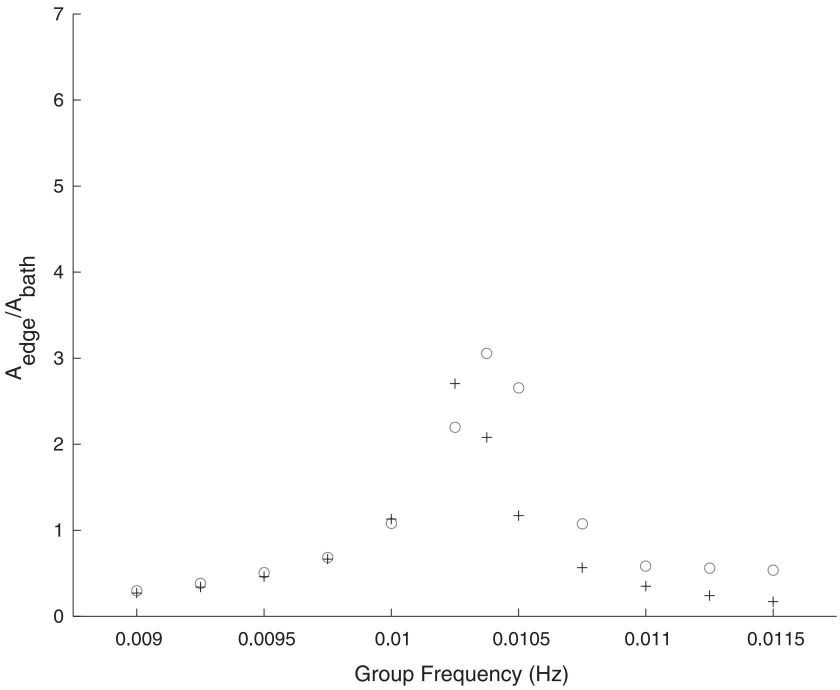

Fig. 5. Edge wave amplitudes with doubled bottom friction. All other quantities remain the same as Fig. 4.

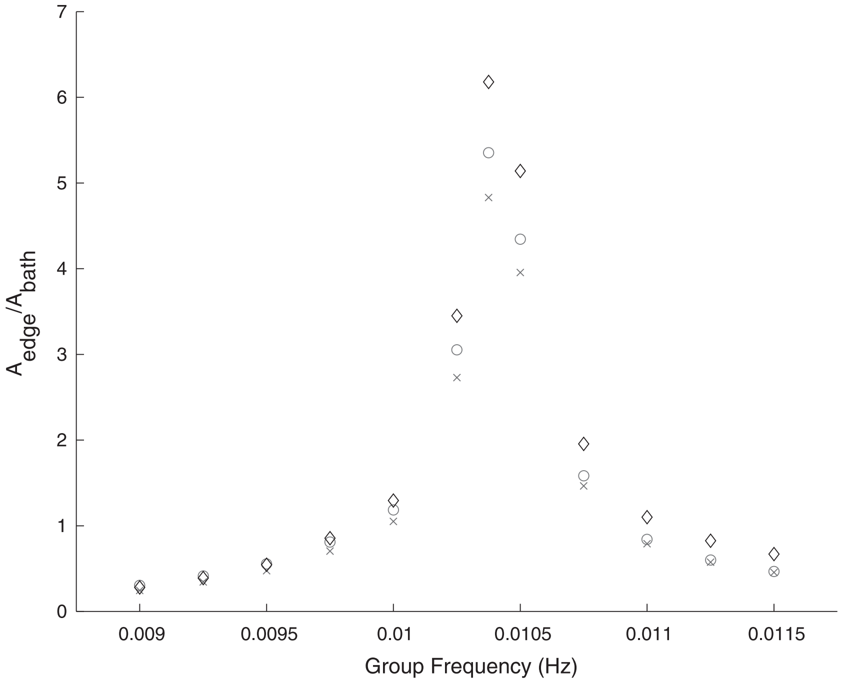

Fig. 6. Edge wave amplitudes using different definitions of mode shape. ◇: using Eq. (75); ○: using perturbed bathymetry, no setup; ×: using perturbed bathymetry with setup.

figures (Figs. 4 and 5) used mode shapes and frequencies computed with the perturbed bathymetry and the still water level (see Appendix A). Alternatives would be to use mode shapes computed using the perturbed bathymetry and mean setup to provide water depths, or to use the planar edge wave mode shape (Eq. (75)). Although all of the mode shapes looked very similar to the eye, quantitative amplitudes differed. Fig. 6 shows results for all three edge wave definitions with a wave height $H_{RMS} = 1.0$ m and low bottom friction (as in Fig. 4). Amplitudes vary by as much as 30%, showing that the assumptions used to define edge waveshape can have a strong effect on amplitude estimates. As all three definitions have considerable justification, the correct answer is unclear.

For more realistic field conditions, there will be several differences from our idealisation. Most obviously, waves will not be bichromatic and will instead have a full directional spectrum with a mean angle that will differ from shore normal. Secondly, bathymetric variations will also be irregular in the cross shore and longshore coordinates, and amplitudes will probably be larger than the 1 cm assumed. Field profiles are also unlikely to be planar.

The main result of this will be a spectrum of edge wave generation. Instead of a single resonance peak, edge waves with a variety of modes and periods are likely to be generated, as observed in the field (Oltman-Shay and Guza, 1987). Because almost all edge wave response is near resonance, measured edge wave–frequency relationships will closely resemble free modes. Overall, edge wave energy generated using this mechanism will be strongly dependent on the amplitudes of bathymetric variations. Such broadbanded forcing and response will form the subject of future investigations.

7. Conclusions

The computational wave models introduced here provide a very versatile tool for investigating nearshore hydrodynamics. In comparison to earlier nearshore models for use with coupled wave–current systems, they offer unsteady refraction, diffraction, shoaling and breaking on ambient currents. Both unsteady wave forcing and unsteady currents are incorporated into the model. Modifications ensure that the system can be well defined even in areas where many simpler models would fail—i.e. where caustics exist.

The computational test on the BBR shoal, verified by comparison with experimental data, shows that good accuracy can be achieved with a reasonable computational cost. This will allow for the simulation of unsteady nearshore hydrodynamics on field scales and times, for a wide variety of conditions. The second computational test showed that wave groups could be responsible for significant edge wave generation whenever there are topographic nonuniformities. This is a fundamentally unsteady result that could never be examined using steady forcing.

In infinite depth, and for finite depth flat beds, the theory which parallels the present study is more developed. Nonlinear Schrödinger and Davey–Stewartson equations have been well studied, partly in order to examine the stability properties and because analytic solutions are available for 1DH in terms of inverse scattering transforms (Zakharov and Shabat, 1972). In addition, the unsteady behavior of wave trains which approach the limit of the narrowband approximation has been examined by Osborne et al. (2000). Higher-order equations are available for both higher-order nonlinearity (e.g. Lo and Mei, 1987) and broader bandwidth (Trulsen and Dysthe, 1996). An extension of the present theory to broader bandwidth in spatial modulations would lead to a model paralleling the higher-order parabolic model of Kirby (1986) and others and should be undertaken in the future.

Acknowledgements

This work was supported by the National Ocean Partnership Program (NOPP), grant N00014-99-1-1051, and by the University of Florida.

Appendix A. Computing eigenmodes of an irregular basin

An irregularly shaped basin with varying depths will resonate with a wide range of frequencies and eigenmodes. If the linear shallow water equations are used to describe fluid motion, then, for a given topography, motion of any eigenmode may be described by

$$h_x\eta_x + h_y\eta_y + h\eta_{xx} + h\eta_{yy} = -\frac{\omega^2}{g}\eta \tag{78}$$

The problem then becomes one of identifying eigenmodes $\eta(x, y)$ and eigenvalues $-\omega^2/g$ satisfying this equation. Discretising all surface elevations by second-order central differences at some typical point (i, j) yields an equation

$$\begin{aligned}\eta_{(i,j)}\left[-2h_{(i,j)}\left(\frac{1}{\Delta x^2}+\frac{1}{\Delta y^2}\right)\right]+\eta_{(i-1,j)}\left[\frac{-h_{x(i,j)}}{2\Delta x}+\frac{h_{(i,j)}}{\Delta x^2}\right]\\ +\eta_{(i+1,j)}\left[\frac{h_{x(i,j)}}{2\Delta x}+\frac{h_{(i,j)}}{\Delta x^2}\right]+\eta_{(i,j-1)}\left[\frac{-h_{y(i,j)}}{2\Delta y}+\frac{h_{(i,j)}}{\Delta y^2}\right]\\ +\eta_{(i,j+1)}\left[\frac{h_{y(i,j)}}{2\Delta y}+\frac{h_{(i,j)}}{\Delta y^2}\right]=-\frac{\omega^2}{g}\eta_{(i,j)}\end{aligned} \tag{79}$$

When this is performed at every point, a large sparse matrix equation results. The eigenvectors and eigenvalues of the matrix give orthogonal solutions to the original equation and are the free oscillation modes and negative squares of the radial frequencies.

It is easiest to set up the system in a rectangular domain, although the basin itself does not need to be rectangular. After setting up a bathymetry in a rectangular matrix, dry points may simply be given dummy equations, while symmetry or periodicity may be used to provide boundary conditions for wet points adjacent to dry points or at the boundaries of the rectangular domain.

Once the system is set up, eigenvectors and eigenvalues may be easily found using any of a number of commercial packages for sparse matrices. Usually, it is the lowest eigenvalues that are of most interest, as these represent the fundamental basin modes and frequencies.

References

Allen, J.S., Newberger, P.A., Holman, R.A., 1996. Nonlinear shear instabilities of alongshore currents on plane beaches. J. Fluid Mech. 310, 181–213.

Berkhoff, J.C.W., 1972. Computation of combined refraction–diffraction. Proc. 13th Intl. Conf. Coast. Engrng., pp. 471–490. Vancouver.

Berkhoff, J.C.W., Booy, N., Radder, A.C., 1982. Verification of numerical wave propagation models for simple harmonic linear water waves. Coast. Eng. 6, 255–279.

Bowen, A.J., 1969a. The generation of currents on a plane beach. J. Mar. Res. 27, 206–215.

Bowen, A.J., 1969b. Rip currents 1. Theoretical investigations. J. Geophys. Res. 74, 5467–5478.

Bowen, A.J., Holman, R.A., 1989. Shear instabilities of the mean longshore current: 1. Theory. J. Geophys. Res. 94, 18023–18030.

Chen, Q., Dalrymple, R.A., Kirby, J.T., Kennedy, A.B., Haller, M.C., 1999. Boussinesq modelling of a rip current system. J. Geophys. Res. 104, 20617–20637.

Chu, V., Mei, C.C., 1970. On slowly varying Stokes' waves. J. Fluid Mech. 41, 873–887.

Dalrymple, R.A., Lozano, C.J., 1978. Wave–current interaction models for rip currents. J. Geophys. Res. 83, 6063–6071.

Davey, A., Stewartson, K., 1974. On three-dimensional packets of surface waves. Proc. R. Soc. Lond. A 338, 101–110.

Foda, M.A., Mei, C.C., 1981. Nonlinear excitation of long-trapped waves by a group of short swells. J. Fluid Mech. 111, 319–345.

Gallagher, B., 1971. Generation of surf beat by non-linear wave interactions. J. Fluid Mech. 49, 1–20.

Guza, R.T., Davis, R.E., 1974. Excitation of edge waves by waves incident on a beach. J. Geophys. Res 79, 1285–1291.

Haller, M.C., Dalrymple, R.A., 2001. Rip current instabilities. J. Fluid Mech. 433, 161–192.

Henderson, S.M., Bowen, A.J., 2002. Simulations of dissipative, shore-oblique infragravity waves. Submitted for publication.

Kirby, J.T., 1986. Higher-order approximations in the parabolic equation method for water waves. J. Geophys. Res. 91 (C1), 933–952.

Kirby, J.T., Dalrymple, R.A., 1983. A parabolic equation for the combined refraction/diffraction of Stokes waves by mildly-varying topography. J. Fluid Mech. 136, 453–486.

Kirby, J.T., Dalrymple, R.A., 1984. Verification of a parabolic equation for propagation of weakly nonlinear waves. Coast. Eng. 8, 219–232.

Kirby, J.T., 1986. An approximate model for nonlinear dispersion in monochromatic wave models. Coast. Eng. 9, 545–561.

Lippmann, T.C., Holman, R.A., Bowen, A.J., 1997. Generation of edge waves in shallow water. J. Geophys. Res. 102, 8663–8679.

Liu, P.L.-F., Dingemans, M.W., 1989. Derivation of the third-order evolution equations for weakly nonlinear water waves propagating over uneven bottoms. Wave Motion 11, 42–64 (Errata by Huang, H., Zhou, X., and Ding, P. (2001), Wave Motion, 33, 209–210).

Lo, E., Mei, C.C., 1987. A numerical study of water-wave modulation based on a higher-order nonlinear Schrödinger equation. J. Fluid Mech. 150, 395–416.

Longuet-Higgins, M.S., 1970a. Longshore currents generated by obliquely incident sea waves, 1. J. Geophys. Res. 75, 6778–6789.

Longuet-Higgins, M.S., 1970b. Longshore currents generated by obliquely incident sea waves, 2. J. Geophys. Res. 75, 6790–6801.

Longuet-Higgins, M.S., Stewart, R.W., 1964. Radiation stresses in water waves; a physical discussion, with applications. Deep-Sea Res. 11, 529–562.

Lozano, C., Liu, P.L.-F., 1980. Refraction–diffraction model for linear surface water waves. J. Fluid Mech. 101, 705–720.

Nwogu, O., 1993. Alternative form of Boussinesq equations for nearshore wave propagation. J. Waterw. Port Coast. Ocean Eng. 119, 618–638.

Oltman-Shay, J., Guza, R.T., 1987. Infragravity edge wave observations on two California beaches. J. Phys. Oceanogr. 17, 644–663.

Osborne, A.R., Onorato, M., Serio, M., 2000. The nonlinear dynamics of rogue waves and holes in deep-water gravity wave trains. Phys. Lett., A 275, 386–393.

Özkan-Haller, H.T., Kirby, J.T., 1999. Nonlinear evolution of shear instabilities of the longshore current: a comparison of observations and computations. J. Geophys. Res. 104, 25953–25984.

Özkan-Haller, H.T., Vidal, C., Losada, I.N., Medina, R., Losada, M.A., 2001. Standing edge waves on a pocket beach. J. Geophys. Res. 106, 16981–16996.

Peregrine, D.H., 1998. Surf zone currents. Theor. Comput. Fluid Dyn. 10, 295–309.

Radder, A.C., 1979. On the parabolic equation method for water-wave propagation. J. Fluid Mech. 95, 159–176.

Schäffer, H.A., 1993. Infragravity waves induced by short wave groups. J. Fluid Mech. 247, 551–588.

Schäffer, H.A., 1994. Edge waves forced by short-wave groups. J. Fluid Mech. 259, 125–148.

Svendsen, I.A., 1984. Mass flux and undertow in a surf zone. Coast. Eng. 8, 347–365.

Svendsen, I.A., Haas, K., Zhao, Q., 2002. Quasi-3D nearshore circulation model SHORECIRC. Version 2.0, Research Report CACR-02-01, Center for Applied Coastal Research, University of Delaware, Newark.

Trulsen, K., Dysthe, K.B., 1996. A modified nonlinear Schrödinger equation for broader bandwidth gravity waves on deep water. Wave Motion 24, 281–299.

Turpin, F.-M., Benmoussa, C., Mei, C.C., 1983. Effects of slowly varying depth and current on the evolution of a Stokes wave packet. J. Fluid Mech. 132, 1–23.

Wei, G., Kirby, J.T., Grilli, S.T., Subramanya, R., 1995. A fully nonlinear Boussinesq model for surface waves: I. Highly nonlinear, unsteady waves. J. Fluid Mech. 294, 71–92.

Zakharov, V.E., Shabat, A.B., 1972. Exact theory of 2-dimensional self-focusing and one-dimensional self-modulation of waves in nonlinear media. Sov. Phys. JETP-USSR 34, 62.